2008 American Control Conference
Westin Seattle Hotel, Seattle, Washington, USA
June 11-13, 2008

Control Input Separation Methods Applied to Cavity Flow

Coşku Kasnakoğlu, Edgar Caraballo, Andrea Serrani and Mo Samimy

Abstract— **Two control input separation methods for control-oriented reduced-order modeling of flow systems are developed and implemented in a cavity flow experimental facility. The proposed methods are 1) actuated POD expansion with stochastic estimation and 2) optimization on a Hilbert space, respectively. These methods extend the baseline flow model through the use of innovation vectors, which capture the distance of the actuated flow from the baseline space. This technique remedies certain gaps associated with the sub-domain separation method employed in our earlier works by 1) producing models that exactly reduce to baseline case under no input, 2) not requiring an identifiable control region and 3) improving the estimation of the control terms. The methods are evaluated in experiments to test their ability to achieve reconstruction of the flow. Also, the performance of closed loop controllers built from models based on these new techniques are analyzed. It is seen that these controllers perform satisfactorily in terms of resonance peak suppression, and compare favorably over the old one in terms of power consumption.**

I. Introduction

It is typical for flow control problems that the control input is applied from the physical boundaries of the system. Control of the flow over a shallow cavity is a benchmark example of boundary flow control that is of great interest due to its rich nature and many applications. Cavity flow is characterized by a strong coupling between flow dynamics and acoustics that produces a self-sustained resonance, which is known to cause, among other problems, structural fatigue in weapons bays. The problem of suppressing cavity flow resonance has been researched extensively in the literature, see for instance [1]–[3] which include the work of our flow control group at the Gas Dynamics and Turbulence Lab (GDTL) at The Ohio State University (OSU). Having obtained controllers that work successfully in physical experiments, we are currently working on improving our designs and establishing stronger theoretical foundations for the key components of our approach. Towards this goal, we have identified control input separation as one such component in need of improvement. Some previous work on input separation issues includes techniques such as lifting, weak formulation, balanced truncation, and control functions [4]–[6]. As for our group, in the past we developed and used the so-called sub-domain separation method (see [7], [8].) There are however, some major issues associated with the sub-domain method: First of all, when the separation is performed after the generation of a POD basis from actuated flow, the model does not reduce itself to the unforced baseline case when the input vanishes. Another issue is the requirement to identify a control region, which can be difficult or impossible in some applications. Finally, a mismatch between the model used for simulation and control design and the behavior of the controlled plant has been typically observed in experiments, due to underestimation of the control vector field in the reduced-order model.

In this paper, we propose two control input separation methods that address in part these issues, and present the results obtained on the cavity flow experimental facility at OSU GDTL. Specifically, in Section II we present some motivations behind this work. The new separation approaches are described in detail in Section III. Experimental results on velocity reconstruction and feedback control of cavity flows are discussed in Section IV. Finally, Section V provides some concluding remarks.

This work is supported in part by AFOSR and AFRL/VA through the Collaborative Center of Control Science (Contract F33615-01-2-3154).

C. Kasnakoğlu is with the Electrical and Electronics Engineering Department at TOBB University of Economics and Technology, 06560 Ankara, Turkey. A. Serrani is with the Department of Electrical and Computer Engineering at The Ohio State University, Columbus, OH 43210, USA. E. Caraballo and M. Samimy are with the Department of Mechanical Engineering at The Ohio State University, Columbus, OH 43210, USA. Corresponding author: Andrea Serrani (serrani@ece.osu.edu)

II. Motivations and Background

In this section, we will first provide a brief summary of the classical POD/GP approach to reduced-order modeling of cavity flow; we then present the sub-domain approach used previously to achieve control input separation.

A. Classical POD/GP Based Modeling

The dynamics of the cavity flow process over a domain $\Omega \in \mathbb{R}^2$, is described by the compressible Navier-Stokes equations governing the spatio-temporal evolution of the flow velocity in the stream-wise and vertical direction, $\boldsymbol{u}(x,t) = (u(x,t), v(x,t))$, and the local speed of sound, $c(x,t)$. These equations can be expressed in compact form as the evolutionary equation

$$\dot{q} = X(q) := C + L(q) + Q(q,q) \tag{1}$$

where $q := (u, v, c)$ is the augmented flow velocity, C is a constant, $L(q)$ is linear in q, and $Q(q,q)$ is quadratic in q [9]. Let $\mathbb{H}$ be a real Hilbert space with inner product $\langle \cdot, \cdot \rangle : \mathbb{H} \times \mathbb{H} \to \mathbb{R}$ such that $q : \Omega \times \mathbb{R}_+ \to \mathbb{R}^3$, $q(\cdot, t) \in \mathbb{H}$, $q(x, \cdot) \in \mathcal{C}^k$ and $k \in \mathbb{N}$. Let $q_k(x) = q(x, t_k)$ be a *snapshot* taken at time t_k and let $\{q_k\}_{k=1}^M \subset \mathbb{H}$ be an ensemble of $M \in \mathbb{N}$ snapshots collected at times $\{t_k\}_{k=1}^M$. Let $q_0 := E[q_j]$ where E is a linear averaging operation $E[q_j] = M^{-1} \sum_{i=1}^M w_j q_j$ for some weights w_j. From the snapshots $\{q_k\}_1^M$, the POD procedure is used to obtain a set of *POD modes* $\{\phi_i\}_1^N \subset \mathbb{H}$

a set of *time coefficients* $\{a_i\}_1^N \subset \mathbb{R}$ so that[1]

$$q(x,t) \approx q_0 + \sum_{i=1}^{N} a_i(t)\phi_i(x) \ . \tag{2}$$

A dynamical system that approximates the flow dynamics can be obtained by Galerkin projection as $\dot{r} = X_S(r)$, where $r := q_0 + a_j\phi_j \in S$, and $S := q_0 + \text{span}\{\phi_1, \ldots, \phi_n\}$. Simplification yields the set of nonlinear ODEs

$$\dot{a}_k = \langle X(r), \phi_k \rangle \ , \qquad k = 1 \ldots N. \tag{3}$$

Note that, at this stage, the effect of actuation is still buried into the Galerkin system coefficients and does not appear explicitly in (3). To remedy this situation, the so-called sub-domain separation method has been employed in our previous work (see [3]).

B. Sub-domain Separation Method (M0)

The idea behind the sub-domain method is to divide the entire flow domain Ω into two sub-regions, so that $\Omega = \Omega_1 \cup \Omega_2$. The smaller domain Ω_1 comprises the physical region where the actuation enters the flow field. Separation is performed at the level of the Galerkin projection by splitting the inner product as $< \cdot, \cdot >_\Omega = < \cdot, \cdot >_{\Omega_1} + < \cdot, \cdot >_{\Omega_2}$. The boundary conditions are imposed on Ω_1. This procedure yields a non-autonomous set of ODEs in the following form

$$\dot{a}_k = F_k + G_{1ik}a_i + g_{2k}\gamma + H_{1ijk}a_ia_j + H_{2ik}a_i\gamma$$

where γ is the input signal (for instance, the voltage applied to a synthetic jet-like actuator). Further details on this method and its application to the cavity flow control problem can be found in [3], [7], [10]. In our work, it was observed that the M0 method suffers from issues such as mismatch with the baseline model, a need for an identifiable control region and the underestimation of the effect of control. These undesirable effects lead us to develop and apply alternative separation methods, as described in the following section.

III. Alternative Separation Approaches

Two approaches to input separation, alternative to sub-domain techniques, have been considered: 1) POD expansion on actuated flow followed by stochastic Estimation (M1) and 2) $\mathcal{L}_2$-optimization (M2). We start by defining concepts that are common to both approaches; then, we explain each approach in detail and comment on their differences.

A. Basic concepts

Both approaches rely on an expansion of the flow field in terms of *baseline POD modes* and *actuation modes*. The baseline modes $\phi_i^{\text{b}}(x)$ are to be extracted from the unactuated flow (i.e. the $\gamma = 0$ case, termed 'B' for 'baseline' or 'nc' for 'no control') using standard POD as explained in Section II-A. The *innovation* is defined as $\tilde{q}(x,t) := q(x,t) - P_S q(x,t)$, where $S := q_0 + \text{span}\{\phi_i^b\}$ and P_S is the projection operator onto S. Forced flow snapshots are projected onto the span

[1]Whenever convenient, we will use Einstein notation to omit summation signs and write $q(x,t) \approx q_0 + a_i(t)\phi_i(x)$ in place of (2).

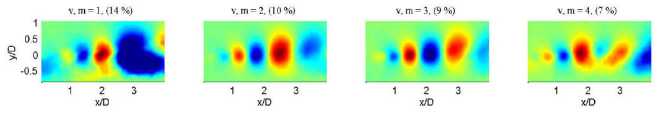

Fig. 1. Baseline POD modes.

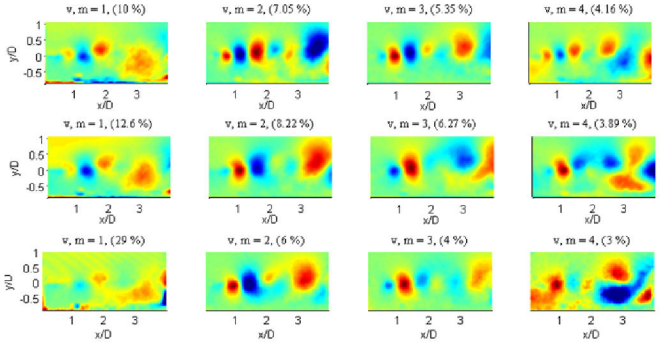

Fig. 2. Control modes for M1 based on different forcing conditions; a) F4 forcing, b) combination of F1 and F4 , and c) white noise forcing.

of the baseline POD modes to obtain the portion of the controlled flow that is recovered by S. The innovation yields the information which is not captured by S and is due to the effect of the actuation. The actuation modes are built from the innovation using one of the methods described next.

B. POD Expansion on Actuated Flow and Stochastic Estimation (M1)

The method M1 can be described as follows: Once the baseline POD modes ϕ_i^b, and the innovations $\tilde{q}_i$ are built, one seeks to find an expansion of the flow field in the form

$$q(x,t) \approx q_0(x) + \sum_{i=1}^{N} \phi_i^{\text{b}}(x)a_i^{\text{b}}(t) + \sum_{i=1}^{N_{ac}} \psi_i^{\text{ac}}(x)a_i^{\text{ac}}(t) \tag{4}$$

where ψ_i^{ac} are actuation modes which are determined using the POD procedure described in Section II-A, but this time applied to snapshots of the innovation $\tilde{q}_i$. The Gram-Schmidt procedure is then used to make sure that the actuation modes are orthonormal to one another and to the baseline modes. Figure 2 shows the control modes $\{\psi_i^{\text{ac}}\}_{i=1}^{N_{ac}}$ for $N_{ac} = 4$ computed under three different actuation: F4, F4 & F1 combined, and white noise (see Table II for details on the nomenclature). The next step is the correlation of the forcing input γ with the actuation mode coefficients a_i^{ac} in (4). For this purpose, we use a second-order stochastic estimation method. The voltage input to the actuator is the natural choice to estimate the amplitude of the control mode coefficients a_i^{ac}, as it captures the actual control signal sent into the system. This variable is dictated by the control system only and corresponds to the open-loop voltage or the signal fed back by the closed-loop system. Once the estimation coefficients are determined, the modal amplitude of the control term can be replaced by

$$a_i^{\text{ac}} = M_i\gamma + O_i\gamma^2 \tag{5}$$

where M and O are the estimation vectors for the linear and quadratic portion correspondingly, and γ is the input voltage. Substituting (5) into (4) yields

$$\begin{aligned} q(x,t) \approx & q_0(x) + \phi_i^{\mathrm{b}}(x) a_i^{\mathrm{b}}(t) + \psi_i^{\mathrm{ac}}(x)(M_i\gamma(t) + O_i\gamma(t)^2) \\ \approx & q_0(x) + \phi_i^{\mathrm{b}}(x) a_i^{\mathrm{b}}(t) + \gamma(t)\psi_1(x) + \gamma(t)^2\psi_2(x) \end{aligned} \tag{6}$$

where $\psi_1 := \sum_{i=1}^{N_{ac}} \psi_i^{\mathrm{ac}}(x) M_i$ and $\psi_2 := \sum_{i=1}^{N_{ac}} \psi_i^{\mathrm{ac}}(x) O_i$. This procedure generates a Galerkin model of the form

$$\begin{aligned} \dot{a}_k = & F_k + G_{1ik} a_i + g_{2k}\gamma + H_{1ijk} a_i a_j + H_{2ik} a_i \gamma \\ & + (h_{3k} + g_{3k})\gamma^2 + H_{3ik} a_i \gamma^2 + h_{4k}\gamma^4 + h_{5k}\gamma^3. \end{aligned} \tag{7}$$

C. $\mathcal{L}_2$ optimization (M2)

The second method M2 considers an expansion of the form

$$q \approx q_0 + \sum_{i=1}^{N} a_i \phi_i^b + \gamma\psi \tag{8}$$

where a single actuation mode ψ is to be chosen so as to minimize the energy not captured by such an expansion. The first step is to obtain the baseline POD modes ϕ_i^b, and building the innovations $\tilde{q}_i$ as described in Section III-A. Then, an optimization problem on the Hilbert space $\mathbb{H}$ can be defined as finding $\psi^\star = \arg\min_{\psi\in\mathbb{H}} J(\psi)$, where $J(\psi) := E\left[\|\tilde{q}_k - \gamma_k\psi\|^2\right]$. The element $\psi^* \in \mathbb{H}$ will be chosen as the actuation mode. The squared norm of the velocity represents the energy contained in the flow. Therefore, among all augmented POD expansions in the form given in (8) where *the input γ directly appears as the coefficient of ψ*, the choice $\psi = \psi^*$ is optimal, in the sense that the energy not captured by this expansion achieves its minimum for $\psi = \psi^*$. The theorem below summarizes the main result:

Theorem 1.

1) *The minimum value of the function J is achieved at* $\psi^* = \frac{E[\gamma_k \tilde{q}_k]}{E[(\gamma_k)^2]}$.
2) $\psi^* \in \mathbb{H}$.
3) $\psi^* \perp \phi_i$ *for* $i = 1, \ldots, N$.

Proof. (1) Note that

$$J(\psi) = E\left[\|\tilde{q}_k\|^2 - 2\gamma_k\langle\tilde{q}_k, \psi\rangle + (\gamma_k)^2\|\psi\|^2\right] .$$

Since J is quadratic in ψ with a positive leading coefficient, it has a unique minimum. Computing the first variation of J with respect to $\xi \in \mathbb{H}$ yields

$$\begin{aligned} & \left.\frac{d}{d\delta}\right|_{\delta=0} J(\psi + \delta\xi) = \\ & \left.\frac{d}{d\delta}\right|_{\delta=0} E\left[\|\tilde{q}_k\|^2 - 2\gamma_k\langle\tilde{q}_k, \psi + \delta\xi\rangle + \gamma_k^2\|\psi + \delta\xi\|^2\right] \\ & = \left\langle E\left[-2\gamma_k\tilde{q}_k + 2\gamma_k^2\psi\right], \xi\right\rangle . \end{aligned}$$

For ψ to be an extremum of J, its first variation must vanish $\forall\xi \in \mathbb{H}$. Therefore $E\left[-2\gamma_k\tilde{q}_k + 2\gamma_k^2\psi^*\right] = 0$ and thus, by linearity of E, $\psi^* = \frac{E[\gamma_k\tilde{q}_k]}{E\left[\gamma_k^2\right]}$. (2) The fact that $\psi^* \in \mathbb{H}$ follows from the fact that E is linear, $\gamma_k\tilde{u}_k \in \mathbb{H}$ and $E\left[(\gamma_k)^2\right] \in \mathbb{R}$. (3) To show that $\psi^* \perp \phi_i$ for $i = 1 \ldots N$, first note that $\tilde{q}_k \perp S$ for all $k = 1 \ldots N$. For any i and k,

$$\begin{aligned} \langle\tilde{q}_k, \phi_i\rangle &= \langle q - P_S q, \phi_i\rangle = \langle q - \sum_{j=1}^{n}\langle q, \phi_j\rangle\phi_j, \phi_i\rangle \\ &= \langle q, \phi_i\rangle - \sum_{j=1}^{n}\langle q, \phi_j\rangle\langle\phi_j, \phi_i\rangle = 0 . \end{aligned}$$

Then, for any i, using the above result, the linearity of E and the linearity of the inner product, one obtains

$$\langle\psi^*, \phi_i\rangle = \left\langle \frac{E\left[\gamma_k\tilde{q}_k\right]}{E\left[\gamma_k^2\right]}, \phi_i \right\rangle = \frac{E\left[\gamma_k\left\langle\tilde{q}_k, \phi_i\right\rangle\right]}{E\left[\gamma_k^2\right]} = 0 .$$

Therefore it follows that $\psi^* \perp S$. □

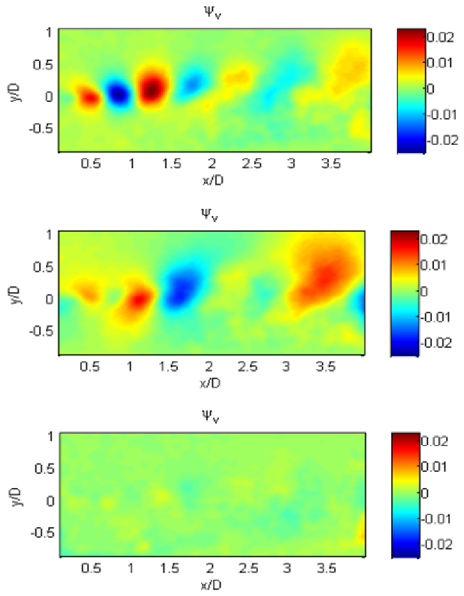

Fig. 3. Control modes for separation method M1, based on different forcing conditions; a) F4 forcing, b) combination of F1 and F4 forcing, and c) White noise forcing.

Criteria	M0	M1	M2
Provides the input γ as a separate term	Yes	Yes	Yes
Requires identification of a control region	Yes	No	No
Consistent with baseline flow for $\gamma = 0$	No	Yes	Yes
Correctly estimates magnitudes of control terms	No	Yes	Yes

TABLE I
COMPARISON OF METHODS

Figure 3 shows the control mode ψ computed under three different actuation: F4, F4 & F1 combined, and white noise. The Galerkin model obtained with M2 has the form

$$\dot{a}_k = F_k + G_{1ik} a_i + g_{2k}\gamma + H_{1ijk} a_i a_j + H_{2ik} a_i \gamma + h_{3k}\gamma^2 .$$

A summary of how the new methods for reduced-order modeling M1 and M2 address the problems and difficulties that were associated with the old sub-domain separation method M0 is given in Table I. Table entries in red indicate undesirable properties.

IV. Experimental Results

For the experiments we utilize the cavity flow setup at OSU GDTL [3]. The depth of the cavity is D = 12.7 mm and the length is L = 50.8 mm for a length to depth aspect ratio L/D = 4. For control the cavity is forced in the shear-layer receptivity region by a 2-D synthetic-jet type actuator issuing at 30 degrees relative to the main flow. The snapshots of the flow field required for the development of the low dimensional model are acquired and processed using a LaVision Inc. PIV system. Flush-mounted Kulite transducers are placed at various locations on the walls of the test section for dynamic surface pressure measurements. For state estimation, dynamic pressure measurements are recorded simultaneously with the PIV measurements using a National Instruments (NI) PCI-6143 S-Series data acquisition board mounted on a Dell Precision Workstation 650. For closed-loop control of the flow, a dSPACE 1103 DSP board connected to the Dell Precision Workstation 650 is used.

A. Flow Field Reconstruction

As a first test of the newly proposed methods, we examined how well the POD expansions augmented with the actuation modes were able to reconstruct flow snapshots from experiments. To ascertain the ability of each model to recover the forced flows, we compare the original velocity field with the reconstructed one using the control modes from both separation methods. For the reconstruction of the velocity field, the control modes from two of the control cases, namely F1-F4 and Wn (see Table II) were used in an attempt to establish the ideal forcing to use in the model reduction process. The velocity fields for the forced cases F1 and F4 are reconstructed using white noise or F1-F4 basis. To this end, we took the following steps: First, the modal amplitude of the baseline portion are obtained by projecting the velocity field (PIV images) of the forced flow onto the baseline basis

$$a_i(t) = \langle q(x,t) - q_0(x), \phi_i(x) \rangle \tag{9}$$

where $q(x,t)$ is the forced flow velocity field, $q_0(x)$ is the mean velocity of the baseline flow and $\phi_i(x)$ are the POD bases of the baseline flow. To add the control effect, the control modes are multiplied by the corresponding voltage γ measured at the time the PIV images were taken. For the M1 separation method, this corresponds to the operation shown in (6), and for M2 it corresponds to (8). Then, we define the averaged error as the mean value of the squared difference between the actual velocity and the reconstructed value

$$e(x) = \sqrt{\frac{1}{M}\sum_{k=1}^{M} \left(q_r(x,t_k) - q(x,t_k)\right)^2}\,. \tag{10}$$

This procedure is applied using the F1-F4 or the Wn control modes to reconstruct the forced cases F1 and F4. Figures 4 and 5 show the mean square error of the reconstruction for the F4 and F1 cases. Figures 4(a) and 5(a) show the mean square error when the flow is reconstructed using the white noise control basis. Similarly, Figures 4(b) and 5(b) show the error for the case based on the combination of the forced cases F1-F4. The figure also contains the mean square error for both separation methods, M1 and M2, and both velocity components. It is clear from both figures that the error levels are lower for the Wn case (a). In this case the error is concentrated in the shear layer region and close to the leading edge. We suspect that this is due to the difference in mean flow, as we are using the baseline mean flow as the overall mean. For the cases based on F1-F4, it can be observed that the error spreads in a larger region midway point the cavity and towards the trailing edge. We believe that the main reason for the difference in the mean error

Name	Explanation
B or nc	Baseline flow (no excitation)
F1	Flow under 1610 Hz open loop forcing
F2	Flow under 1830 Hz open loop forcing
F3	Flow under 3250 Hz open loop forcing
F4	Flow under 3920 Hz open loop forcing
Wn	Flow under bandlimited white noise forcing
Bi	Combination of snapshots of B and i
Bij	Combination of snapshots of B, i and j
MkBi	Model built using method Mk from Bi snapshots.
MkBij	Model built using method Mk from Bij snapshots.
MkBi c	Model MkBi under forcing c
MkBij c	Model MkBij under forcing c

$i, j \in$ {F1,F2,F3,F4,Wn}, $k \in \{0,1,2\}$, $c \in$ {nc,F1,F2,F3,F4,Wn}

TABLE II
NOMENCLATURE

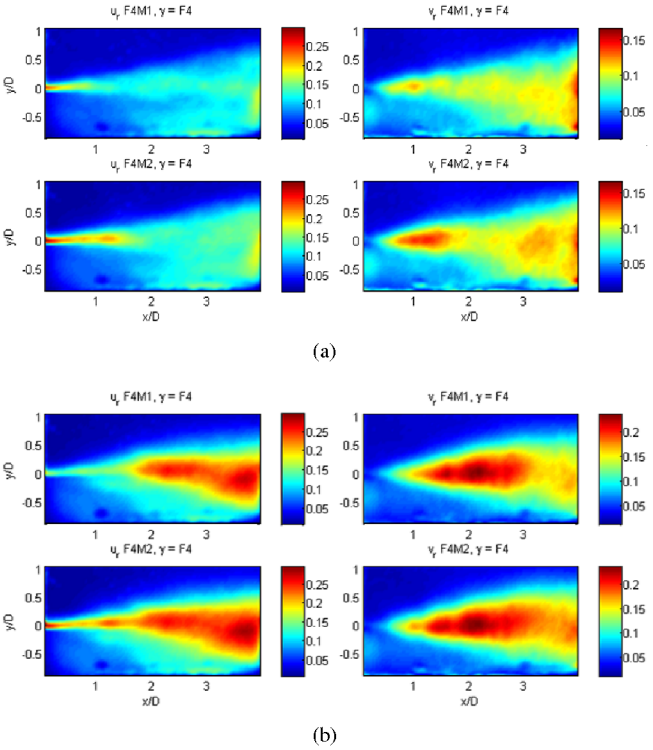

(a)

(b)

Fig. 4. Mean error in the velocity reconstruction for the forced case (F4) for the new models, with the control modes based on: a) white noise forcing (Wn), and b) the combination of F1F4 forcing.

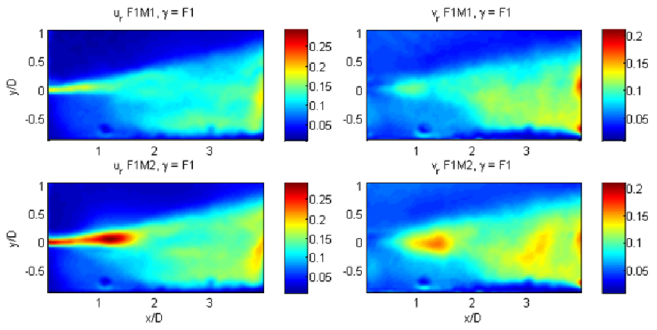

(a)

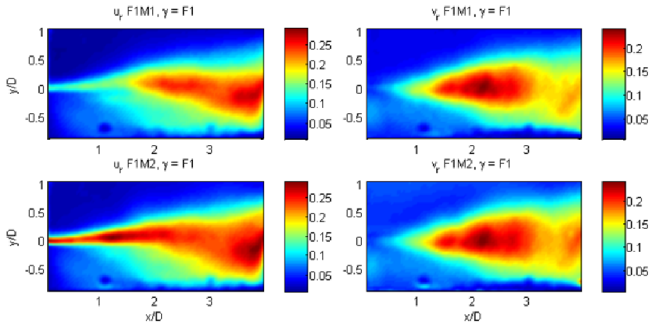

(b)

Fig. 5. Mean error in the velocity reconstruction for the forced case (F1) for the new models, with the control modes based on: a) white noise forcing (Wn), and b) the combination of F1F4 forcing.

is due to the nature of the structures of the control mode basis: for the F1-F4 case, the basis contains large and well organized structures for both models, while the Wn case has more scattered structures. This in turn generates larger fluctuations in the velocity reconstruction when the control portion is introduced. When comparing the effect of the separation method, in either case Wn or F1-F4, there is little difference in the velocity error.

B. Feedback Control Design

After obtaining satisfactory results in velocity reconstruction with the newly developed methods, the new models were used in a feedback control design developed in our earlier works, which has the following steps: 1) state estimation to estimate time coefficients from pressure measurers, 2) LQR control with scaling to achieve reduce oscillations while avoid actuation saturation and 3) actuator compensation to compensate for the unwanted dynamics that the actuator introduces to the system [3]. Controllers are obtained for the seven different models: M0B, M1BF4, M2BF4, M1BF1F4, M2BF1F4, M1BWn, M2BWn. Figure 6 shows the sound pressure level (SPL) reduction obtained by the LQ state feedback control for the different models tested in Mach 0.3 cavity flow for which the models were derived. The thin red line yields the SPL of the unforced baseline flow, whereas the thick line corresponds to the SPL of the flow at the same location under state feedback control. All the models show improvement with respect to the uncontrolled flow by reducing the resonant peak by more than 18 dB,

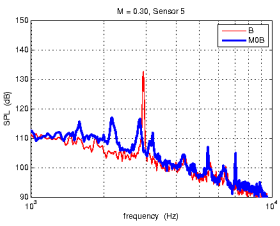

(a) M0B

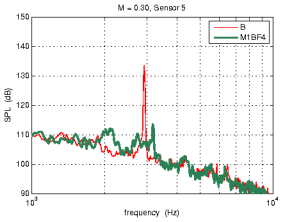

(b) M1BF4

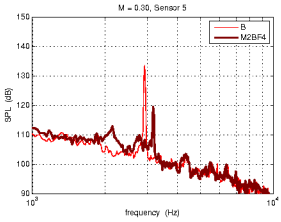

(c) M2BF4

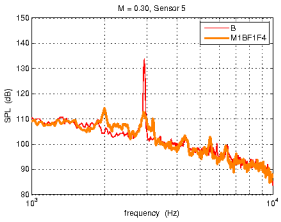

(d) M1BF1F4

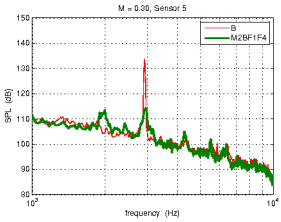

(e) M2BF1F4

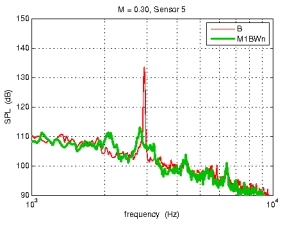

(f) M1BWn

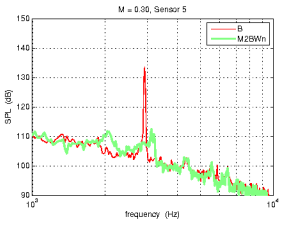

(g) M2BWn

Fig. 6. Sound pressure level (SPL) obtained under LQ control

without the addition of any addition peak. There is not much difference in the SPL results between the models. The performance of the control law was also tested in the closed-loop experiments for an off-design flow condition of Mach 0.32. Figure 7 shows the behavior of the flow under the off design condition for all the models, based on M1 and M2. It can be noticed that in each case the controller is capable of maintaining the same general characteristics and benefits as in the Mach 0.30 design condition. This is consistent with our previous results [3], which showed the robustness of the feedback control loop under off design conditions. Finally in an attempt to quantify the benefits of each model, separation method and flow used to derive the model, we compared the average reduction in the overall sound pressure level (OASPL) calculated using six sensors in the cavity and the mean input voltage used (Vrms). Figure 8 shows the comparison of the different models used for the two Mach numbers tested. The first important observation

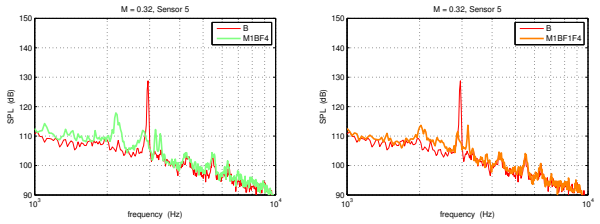

(a) M1BF4 M032

(b) M1BF1F4 M032

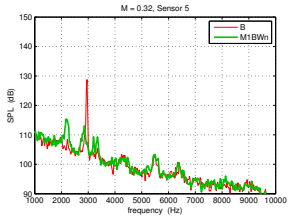

(c) M1BWn M32

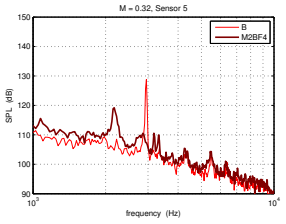

(d) M2BF4 M32

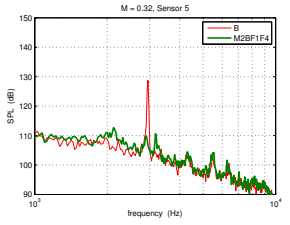

(e) M2BF1F4 M32

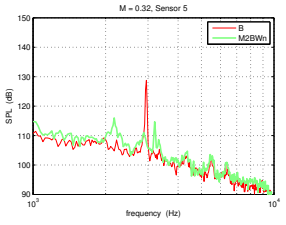

(f) M2BWn M32

Fig. 7. SPL under LQ control for models built with M1 and M2 at the design condition M = 0.30, and at an off design conditions M = 0.32

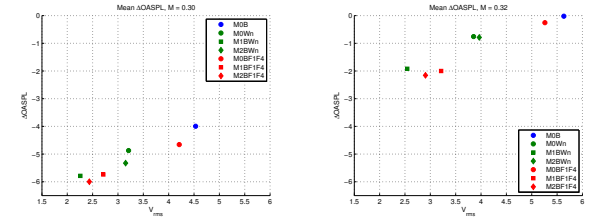

(a) M=0.30

(b) M=0.32

Fig. 8. Rms voltage vs. average OASPL for several models at different Mach numbers: a) M = 0.3 (design condition) b) M =0.32 (off-design condition)

is that models based on the new separation method required less power to achieve similar or better attenuation of the SPL. This is true for both Mach number considered in this study. Secondly, results seem to indicate that the model based on the white noise achieves the best overall performance, noticeably model M1BWn. The model based on M2 seems to perform better for the F1-F4 forcing case; this could be related to small values for the control mode, which in turns require a higher control magnitude to affect the flow.

V. Conclusions

In this paper we presented the development of two new control input separation methods for feedback flow control. The methods incorporate the control input through additional modes obtained from innovation between forced flow and its projection onto the baseline flow. The new methods provide important improvements over the previously developed sub-separation method, such as reducing the model exactly to the baseline under no input, not requiring an identifiable control region, and providing improved estimates for the magnitudes of control derivatives. The new methods were then applied to the OSU GDTL cavity flow experiment where they were evaluated first in their ability to reconstruct actuated flows at the POD level. It was observed that the models improved over existing results in their ability to reconstruct a wide range of flows that are different from the modeling conditions, especially when built from white noise excitation. Next, we tested LQR controllers derived on the basis of the models obtained from the new separation methods. Experimental results showed that these controllers significantly reduce the resonant peak of the single-mode Mach 0.3 flow, for which they were designed, and also performed satisfactorily for off-design conditions at Mach 0.32. This outcome is comparable to what was achieved in previous studies in terms of peak reduction, but is superior in terms of the ratio between overall sound pressure level and mean input voltage.

References

[1] L. N. Cattafesta, D. R. Williams, C. W. Rowley, and F. S. Alvi. Review of active control of flow-induced cavity resonance. In *33rd AIAA Fluid Dynamics Conference*, Orlando, FL, 2003.

[2] C.W. Rowley and D.R. Williams. Dynamics and control of high-reynolds-number flow over open cavities. *Annual Review of Fluid Mechanics*, 38:251–276, 2006.

[3] M. Samimy, M. Debiasi, E. Caraballo, A. Serrani, X. Yuan, J. Little, and J. H. Myatt. Feedback control of subsonic cavity flows using reduced-order models. *Journal of Fluid Mechanics*, 579:315–346, 2007.

[4] M. Hogberg, T. R. Bewley, and D. S. Henningson. Linear feedback control and estimation of transition in plane channel flow. *Journal of Fluid Mechanics*, 481:149–175, 2001.

[5] R Chris Camphouse. Boundary feedback control using Proper Orthogonal Decomposition models. *Journal of Guidance, Control, and Dynamics*, 28:931–938, 2005.

[6] D.A. Lawrence, J.H. Myatt, and R.C. Camphouse. On model reduction via empirical balanced truncation. In *Proceedings of the 2005 American Control Conference*, pages 3139– 3144, Portland, Oregon, 2005.

[7] M. O. Efe and H. Ozbay. Low dimensional modelling and Dirichlet boundary controller design for Burgers equation. *International Journal of Control*, 77(10):895–906, July 2004.

[8] E. Caraballo, X. Yuan, J. Little, M. Debiasi, P. Yan, A. Serrani, J. Myatt, and M. Samimy. Feedback control of cavity flow using experimental based reduced order model. In *Proceedings of the 35th AIAA Fluid Dynamics Conference and Exhibit*, Toronto, ON, 2005. AIAA Paper 2005-5269.

[9] C. W. Rowley, T. Colonius, and R. M. Murray. Model reduction for compressible flows using POD and Galerkin projection. *Physica D*, 189(1-2):115–29, 2004.

[10] E. Caraballo, J. Little, M. Debiasi, and M. Samimy. Development and implementation of an experimental based reduced-order model for feedback control of subsonic cavity flows. *Journal of Fluids Engineering*, 129:813–824, 2007.